An Analysis of ENSO Prediction Skill in the CFS Retrospective Forecasts

RENGUANG WU

Center for Ocean–Land–Atmosphere Studies, Calverton, Maryland

BEN P. KIRTMAN

Rosenstiel School of Marine and Atmospheric Sciences, University of Miami, Miami, Florida, and Center for Ocean–Land–Atmosphere Studies, Calverton, Maryland

HUUG VAN DEN DOOL

Climate Prediction Center, National Centers for Environmental Prediction, Camp Springs, Maryland

(Manuscript received 8 April 2008, in final form 25 September 2008)

ABSTRACT

The present study documents the so-called spring prediction and persistence barriers in association with El Niño–Southern Oscillation (ENSO) in the National Centers for Environmental Prediction (NCEP) Climate Forecast System (CFS) retrospective forecasts. It is found that the spring prediction and persistence barriers in the eastern equatorial Pacific sea surface temperature (SST) are preceded by a boreal winter barrier in the western equatorial Pacific zonal wind stress. The time of the persistence barrier is closely related to the time of the ENSO phase transition, but may differ from the time of the lowest variance. The seasonal change of the signal-to-noise ratio cannot explain the persistence barrier. While the noise may lead to a drop of skill around boreal spring in the western equatorial Pacific zonal wind stress, its impacts on the skill of eastern equatorial Pacific SST is small. The equatorial Pacific zonal winds display an excessive response to ENSO-related SST anomalies, which leads to a longer persistence in the equatorial Pacific thermocline depth anomalies and a delayed transition of the eastern equatorial Pacific SST anomalies. This provides an interpretation for the prediction skill drop in boreal spring in the eastern equatorial Pacific SST. The results suggest that improving the atmospheric model wind response to SST anomalies may reduce the spring prediction barrier.

1. Introduction

El Niño–Southern Oscillation (ENSO) is a coupled ocean–atmosphere phenomenon in the tropical Pacific. It involves interactions among sea surface temperature (SST), thermocline depth, atmospheric convection, and surface winds (Zebiak and Cane 1987; Philander 1990). ENSO events exert substantial impacts on short-term climate variability on the globe. Considerable efforts have been made to improve ENSO forecasts and to understand the physical processes that limit its predictability.

A well-known feature in ENSO forecasts is a significant drop in prediction skill during boreal spring (Goswami and Shukla 1991; Barnston et al. 1994; Balmaseda et al. 1994; Xue et al. 1994; Latif et al. 1998; Kirtman et al. 2001; Schneider et al. 2003; DeWitt 2005; Jin et al. 2008; Jin and Kinter 2009), particularly in terms of eastern Pacific SST correlation coefficients. This spring prediction barrier has been attributed to the low variance of Niño-3 SST anomalies in boreal spring (Xue et al. 1994; Torrence and Webster 1998; Clarke and Van Gorder 1999). The physical argument works as follows: In the spring season, the Walker circulation is weak and the east–west sea level pressure and SST gradient along the equatorial Pacific is at a minimum (Webster and Yang 1992; Webster 1995; Lau and Yang 1996). Under such conditions, the initial errors and ''weather'' noise in the models can project strongly onto ENSO modes, leading to large error growth and deteriorating the forecasts (Blumenthal 1991; Moore and Kleeman 1996). Reducing errors in the initial conditions due to inaccuracies in

Corresponding author address: Renguang Wu, COLA, IGES, 4041 Powder Mill Rd., Suite 302, Calverton, MD 20705.
E-mail: renguang@cola.iges.org

DOI: 10.1175/2008JCLI2565.1

observations and deficiencies in the models could help to improve the forecasts across the spring (Chen et al. 1995, 1997; Kirtman et al. 1997; Schneider et al. 2003). Chen et al. (1995) suggested that the spring predictability barrier is not intrinsic to the real climate system and that it may be a problem of the models. Jin and Kinter (2009) indicated that systematic model errors are major factors limiting the predictability and degrading the forecast skill.

There is a relevant statistical argument, which is indicated in Branstator (1986) and Van den Dool and Toth (1991). The signal is capped by the natural variability, so everything else being the same the signal-to-noise ratio for SST tends to be the lowest in spring. This is similar to numerical weather prediction scores being lower in summer than in winter. The initial error (absolute) may be the same in summer and winter, but in a relative sense this means a larger error in summer as expressed by a lower anomaly correlation (which measures signal to noise ratio) right from the start. This is also similar to scores being higher in strong ENSO years (a lot of signal) as opposed to weaker and neutral years when the signal is weak and the root-mean-square error is not lower. By this statistical argument the spring barrier is intrinsic. While additional observations help (in all seasons) it cannot negate the low signal in spring.

Corresponding to the spring prediction barrier is a spring persistence barrier in the auto-lag correlation of the ENSO indexes (Troup 1965; Wright 1985; Webster and Yang 1992; Xue et al. 1994; Webster 1995; Torrence and Webster 1998). The spring persistence barrier has been related to the phase transition of ENSO (e.g., Torrence and Webster 1998; Clarke and Van Gorder 1999; Burgers et al. 2005), the seasonal change in the ENSO variance (Xue et al. 1994; Balmaseda et al. 1995; Schneider et al. 2003), and the seasonal change in the signal-to-noise ratio (Webster 1995; Torrence and Webster 1998). Burgers et al. (2005) described the spring barrier as a period in which the instability in the phase velocity of ENSO is the largest. Clarke and Van Gorder (1999) suggested that the boreal spring persistence barrier in the Southern Oscillation (SO) index is due to a purely biennial oscillation. Using coupled model experiments, Yu (2005) showed that the biennial component is one major mechanism responsible for the spring persistence barrier and that interactions between the Pacific Ocean, Indian Ocean, and monsoon could enhance the biennial component of ENSO and thus the persistence barrier.

It has been suggested that the spring prediction barrier could be bridged by including additional observed variations in sea level heights or upper-ocean heat contents in the forecast initialization (Smith et al. 1995; Xue et al. 2000). This bridging effect is due to the fact that the eastern equatorial Pacific heat content anomalies lead the eastern equatorial Pacific SST anomalies by several months (Zebiak and Cane 1987; Zebiak 1989; Balmaseda et al. 1995; Meinen and McPhaden 2000). Consistent with this phase relationship, the equatorial Pacific heat content or warm water volume anomalies display a boreal winter prediction barrier rather than a spring barrier (Balmaseda et al. 1995; McPhaden 2003). In analogy with low Niño-3 SST variance in boreal spring, the equatorial Pacific warm water volume anomalies tend to have small variance in boreal winter (McPhaden 2003). Since equatorial Pacific heat content fluctuations are closely related to surface wind changes in the western equatorial Pacific (Kirtman 1997; Weisberg and Wang 1997a,b; Mayer and Weisberg 1998; Wang et al. 1999), a question is: Is there an associated barrier for the low level winds in that area? Here we show that the western equatorial Pacific surface winds have a persistence barrier around the end of the calendar year and the forecast skill of these winds has an obvious drop in boreal winter.

Our analysis focuses on the operational National Centers for Environmental Prediction (NCEP) Climate Forecast System (CFS; Saha et al. 2006), which has become an important forecast tool. Because of the large impacts of ENSO on climate fluctuations in both the tropics and extratropics, it is important to understand how the CFS performs in terms of tropical Pacific SST. In particular, can the CFS retrospective forecasts capture the persistence barrier as seen in observations? Saha et al. (2006) has shown that the CFS SST forecasts experience a large drop of skill in boreal spring. What are the plausible reasons for the drop of skill? Understanding these questions would benefit a better application of ENSO forecasts made based on the CFS.

Another motivation for the present study is whether the spring persistence barrier or prediction barrier is related to the reduction of signal-to-noise ratio. Torrence and Webster (1998) indicated that the persistence barrier occurs when the noise is large and the signal-to-noise ratio of the system is the lowest. This claim is based on simple statistical models in which the seasonal change of the noise variance is given. This is the opposite of the argument by Van den Dool and Toth (1991), who assume that the noise is fairly constant across seasons, so the signal-to-noise ratio variation mainly reflects the variation in signal strength. The ensemble forecasts of the CFS make it possible to estimate the noise and the signal-to-noise ratio and to test the Torrence and Webster's hypothesis.

The rest of the text is as follows: The data used in the present study are described in section 2. Section 3

documents the prediction barrier in CFS retrospective forecasts. Section 4 examines the relationship of the persistence barrier to the time of phase transitions, the seasonal change of variances, and the seasonal change in the signal-to-noise ratio. Section 5 explores plausible reasons for the prediction barrier. A summary is provided in section 6.

2. Data

The analyses in the present study are based on outputs from the CFS 24-yr retrospective forecasts for the period 1981–2004. The details of the CFS model can be found in Wang et al. (2005) and Saha et al. (2006). Here, only a simple description is provided. The atmospheric component of the CFS is the NCEP Global Forecasting System (GFS) model (Moorthi et al. 2001), which has a spectral triangular truncation of T62 in the horizontal and a finite differencing in the vertical with 64 sigma levels. The oceanic component is the Geophysical Fluid Dynamics Laboratory (GFDL) Modular Ocean Model version 3 (MOM3; Pacanowski and Griffies 1998), which has a zonal resolution of 1°. The meridional resolution is 1/3° between 10°S and 10°N, gradually increasing until 1° at 30°S and 30°N. There are 40 layers in the vertical with 27 layers in the upper 400 m.

Details of the CFS retrospective forecasts can be found in Saha et al. (2006). Here, a simple description is provided. Each of the CFS retrospective forecasts covers a full 9-month period. These retrospective forecasts have been done for all months during the period 1981–2004. The atmospheric initial conditions are from the NCEP Department of Energy (DOE) Reanalysis 2 (Kanamitsu et al. 2002). The oceanic initial conditions are from the NCEP Global Ocean Data Assimilation (GODAS; D. Behringer et al. 2005, personal communication). For retrospective forecasts starting from a specific month, there are 15 atmospheric initial conditions (15 runs) that are partitioned into three segments. The first set uses the five atmospheric initial states of the 9th, 10th, 11th, 12th, and 13th of this month and uses the same pentad ocean initial condition centered on the 11th of the same month. The second set uses the five atmospheric initial states of the 19th, 20th, 21st, 22nd, and 23rd of this month and the same pentad ocean initial condition centered on the 21st of the same month. The third set used the five atmospheric initial states of the 29th and 30th of this month and the 1st, 2nd, and 3rd of the next month and the same pentad ocean initial condition centered on the 1st of the next month. Following protocol as in Saha et al. (2006), for the forecast starting from initial conditions of those days of January and 1, 2, and 3 February, February is considered to be the month of forecast lead zero and March is the month of forecast lead 1, and so on.

The analysis is performed for both ensemble mean forecasts and individual forecasts at different leads using monthly mean data. The results obtained from ensemble mean and individual forecasts are similar. We focus on SST and the 20°C isotherm depth (thermocline depth) in the Niño-3.4 region (5°S–5°N, 170°–120°W), and surface zonal wind stress in the western equatorial Pacific (5°S–5°N, 130°–170°E). These are critical quantities in the ENSO evolution (Zebiak and Cane 1987; McPhaden et al. 1998). One reason for choosing the region 130°–170°E for the zonal wind stress is that this is the transition region between westerly and easterly anomalies around the mature phase of ENSO. The other reason is that wind stress changes in this region lead Niño-3.4 thermocline depth and SST changes. The proxies used for comparison with the CFS retrospective forecasts are SST and thermocline depth from the GODAS and the surface wind stress from the NCEP–DOE Reanalysis 2. Note that these two products are used in the initialization of the CFS retrospective forecasts. Saha et al. (2006) verified SST forecasts against optimum interpolation SST (OISST) version 2 (Reynolds et al. 2002). In the tropical Pacific, SST forecasts verifications against either GODAS or OISST version 2 are very close. We have also performed analyses with SST from the NCEP–DOE Reanalysis 2, the thermocline depth from the Simple Ocean Data Assimilation version 1.2 (SODA1.2; Carton et al. 2000), and the surface wind stress from the Florida State University (Goldenberg and O'Brien 1981). The results are similar and thus are not shown.

3. The prediction barrier

We start with the ENSO prediction skill in the CFS retrospective forecasts. Here, the prediction skill is measured by the correlation coefficient between the CFS ensemble mean forecasts and observations. The prediction skill is calculated based on area-mean anomalies. Figure 1 shows the prediction skills for the Niño-3.4 (5°S–5°N, 170°–120°W) SST, Niño-3.4 thermocline depth, and the western equatorial Pacific (5°S–5°N, 130°–170°E) zonal wind stress. These are crucial quantities in the coupled processes of ENSO (Zebiak and Cane 1987; Neelin et al. 1994; McPhaden et al. 1998). Note that the prediction skill for Niño-3.4 SST has been shown by Saha et al. (2006, see their Fig. 1).

The Niño-3.4 SST forecast skill has an apparent drop during April–June for forecasts starting before March (Fig. 1a). The lowest forecast skill (less than 0.4) appears in July for forecasts starting from November to

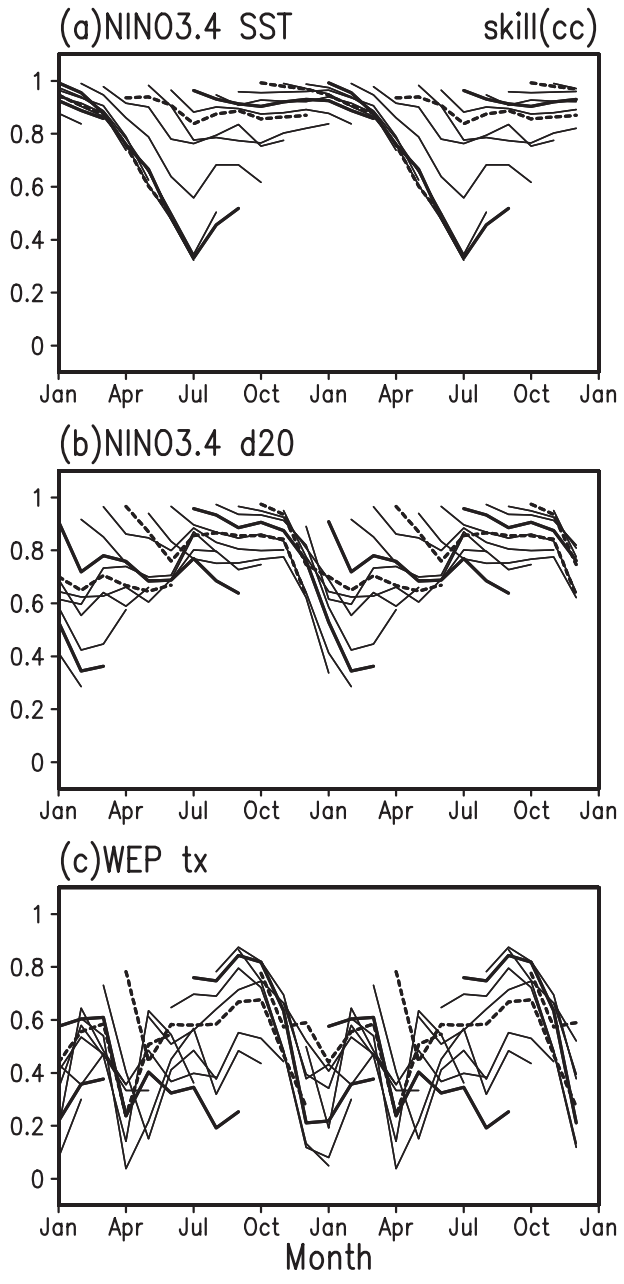

FIG. 1. Correlation skill of (a) Niño-3.4 SST, (b) Niño-3.4 thermocline depth, and (c) western equatorial Pacific zonal wind stress derived from CFS ensemble mean forecasts. For clarity of presentation two repeating years are shown.

January. For forecasts starting after March, the drop of skill is much less with correlations maintained at a high level during November–February. These results are consistent with Saha et al. (2006), and with reported skill by many other methods as well (see Kirtman et al. 2001).

The Niño-3.4 thermocline depth experiences an obvious drop in the forecast skill as well. The deterioration of skill is seen during December–February with the lowest forecast skill appearing in February–March (Fig. 1b), leading the skill drop in the Niño-3.4 SST by about 4–5 months. The time difference of the skill drop between the Niño-3.4 SST and thermocline depth is consistent with their phase lag as shown in previous studies (Zebiak and Cane 1987; Balmaseda et al. 1995). This suggests that the changes in the forecast skill for these two quantities are related. Note that during July–November, the thermocline depth forecast skill remains at the same high level, regardless of forecast lead.

The western equatorial Pacific zonal wind stress shows generally lower skill compared to the Niño-3.4 SST and thermocline depth. There are three periods during which the forecast skill for the wind stress displays obvious drops. The first and most pronounced one is during October–December (Fig. 1c). This one leads the skill drop in the Niño-3.4 thermocline depth by about 1–2 months. In view of the phase relationship between the western equatorial Pacific wind stress and the equatorial Pacific thermocline changes in the ENSO evolution (Wang et al. 1999), this skill drop in the wind stress is likely related to that in the thermocline depth. The second skill drop is seen in March–April, which is likely related to the effects of atmospheric noise. Another skill drop is seen in July–August. Compared to the other two, this latter drop in skill is relatively weak and is only seen for some of the forecasts.

Previous studies have focused on the substantial decrease in observation–prediction correlation in the Niño-3 SST or the SO index across the boreal spring and have attributed the spring prediction barrier to the maximum error growth in boreal spring (e.g., Webster 1995). The forecast skill in Fig. 1 shows that the skill drop in Niño-3.4 thermocline depth and western equatorial Pacific surface wind stress precedes the skill drop in Niño-3.4 SST in boreal spring. This phase relationship suggests that the prediction barrier could be an intrinsic feature of the coupled model (i.e., coupled model error), although the noise may also play a role. This issue will be addressed later (section 5).

To further demonstrate the skill drop, we show in Fig. 2 the correlation calculated at each grid point for the forecasts starting from July and verifying in December. Apparently, the skill for December zonal wind stress is very low over the western equatorial Pacific (Fig. 2c). Corresponding to this, the skill for the January thermocline depth (here thermocline depth in January instead of December is used in view of its time-lag relationship with the western equatorial Pacific wind stress) is relatively low in the equatorial central Pacific around 170°–130°W (Fig. 2b), which is related to the fact that this is the transition region of ENSO-related

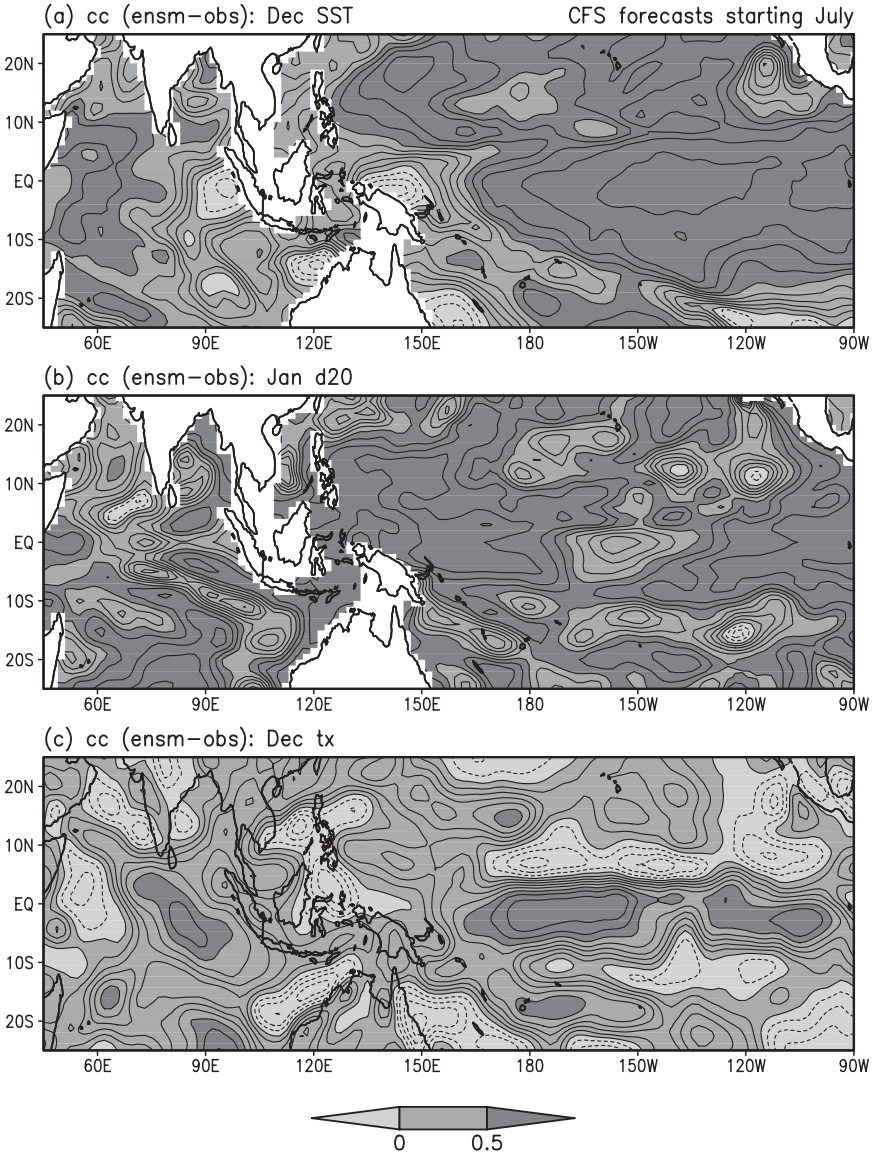

FIG. 2. Correlation skill of (a) December SST, (b) January thermocline depth, and (c) December zonal wind stress derived from CFS ensemble mean forecasts starting from July. The contour interval (CI) is 0.1.

thermocline depth anomalies around the mature phase of ENSO. Note that the SST skill in the central-eastern equatorial Pacific is very high at the same time (Fig. 2a). In contrast, the SST skill in the western equatorial Pacific is very low. The high thermocline depth skill in the western and eastern equatorial Pacific could be related to the high skill of zonal wind stress over the equatorial central Pacific during the developing stage of ENSO (see Fig. 10h) through propagation of oceanic waves induced by wind stress and its curl.

As noted above, among the three critical quantities examined, the skill drop in the western equatorial Pacific zonal wind stress in boreal winter is the earliest and could be a precursor for the ENSO SST skill drop in boreal spring. Thus, it is important to understand what causes the low boreal winter skill in the western equatorial Pacific wind stress. East of 150°E, the zonal wind stress shows moderate skill, which is related to its fairly strong dependence on the SST gradient between 140°E and the date line. West of 150°E, low skill is seen for both the wind stress and SST. The spatial collocation of low skill in the wind stress and the SST in the western equatorial Pacific may lead to the speculation that the low skill in local SST may be responsible for the low skill

in wind stress. However, it may also be argued that the low skill in the wind stress could contribute to the low skill in SST since this is a coupled system. As indicated in previous studies, the wind-induced surface evaporation changes can contribute to SST changes in the western-central equatorial Pacific (Wu et al. 2006). It is possible that an initial decrease in the skill of either SST or wind stress is amplified through coupled ocean–atmosphere processes.

The relatively low skill in the western equatorial Pacific zonal wind stress is also seen in the forecasts starting from December (Fig. 3c). The thermocline depth also displays relatively low skill around 150°W (Fig. 3b). Compared to the long-lead forecasts from July, the skill drop is less. This is not surprising since the lead times in Fig. 3 are much less than in Fig. 2. The December SST correlation is very high in the tropics (Fig. 3a) largely because of persistence. As such, the low skill in the western equatorial Pacific wind stress may be contributed by factors other than local SST (i.e., model error or lack of predictability due to SST forcing). We will show later (section 5) that the low skill in the western equatorial Pacific wind stress is in large part due to the improper response of atmospheric winds to ENSO. The differences between the long-lead and short-lead forecasts suggest that coupled processes can amplify the forecast errors and thus enhance the skill drop.

4. The persistence barrier

In close association with the prediction barrier is the persistence barrier. For both the Niño-3 SST and the SO index, the drop in the auto-lag correlation occurs in boreal spring (Webster and Yang 1992; Webster 1995; Clarke and Van Gorder 1999). Understanding the persistence barrier could help to identify the reasons for the prediction barrier. Previous studies have suggested different (but not unrelated) reasons for the spring persistence barrier. Among these are the calendar-locked ENSO phase transition (Lau and Yang 1996; Torrence and Webster 1998; Clarke and Van Gorder 1999; Clarke and Shu 2000; Burgers et al. 2005; Yu 2005), the low variance of the Niño-3 SST anomalies (Xue et al. 1994; Balmaseda et al. 1995), and the lowest signal-to-noise ratio (Webster and Yang 1992; Webster 1995; Torrence and Webster 1998).

In this section, we examine whether the CFS retrospective forecasts display a persistence barrier similar to observations and what is the relationship of the persistence barrier to the time of the phase transition, the seasonal change of the variance, and the signal-to-noise ratio. The analysis has been performed for both ensemble mean forecasts and individual forecasts at different leads based on monthly means. The conclusions drawn from ensemble mean forecasts and individual forecasts are the same. In the following, we only present results based on individual forecasts.

a. The time of persistence barriers

The time of persistence barriers in the CFS forecasts is delayed compared to observations and the delay is more prominent in long-lead (over 3 months) forecasts than in short-lead (0–3 month) forecasts. This is demonstrated in Fig. 4, which shows the auto-lag correlations of Niño-3.4 SST, Niño-3.4 thermocline depth, and the western equatorial Pacific zonal wind stress derived from CFS forecasts and observations. For CFS forecasts, the correlations shown in Fig. 4 are the average of those calculated for each of the 15 individual forecasts. For the observed zonal wind stress, a 3-month running mean has been applied before calculating the correlations.

For Niño-3.4 SST, the drop of the auto-lag correlation is seen during June–July for forecasts starting from December to April (Fig. 4a), which is about 2 month later than observations (Fig. 4d). For forecasts initiated before December, the persistence drop does not show up in the 9-month forecast period. For Niño-3.4 thermocline depth, the decrease in persistence starts around January (Fig. 4b), about 1-month later compared to observations (Fig. 4e). The persistence drop during March–May is larger in the CFS forecasts than in observations. For the western equatorial Pacific zonal wind stress, the forecasts starting from June to September have a longer persistence and the persistence drop occurs after February, about 3-month later compared to observations (Figs. 4c,f). The persistence drop during February–March is also seen for forecasts starting from October to December.

The CFS forecasts capture the time-lag relationship among the persistence barriers of the Niño-3.4 SST, Niño-3.4 thermocline depth, and western equatorial Pacific zonal wind stress. The persistence starts to drop about 4 month earlier in the Niño-3.4 thermocline depth than in the Niño-3.4 SST. The decrease of persistence in the western equatorial Pacific zonal wind stress leads that in the Niño-3.4 thermocline depth persistence by about 1–2 months. These time lags are similar to those seen in the skill drops.

b. The temporal evolution of ENSO-related anomalies

The delay in the persistence drop in the CFS forecasts is related to the delay in the temporal evolution of ENSO-related anomalies. This is illustrated in Fig. 5, which shows the difference of composite El Niño minus

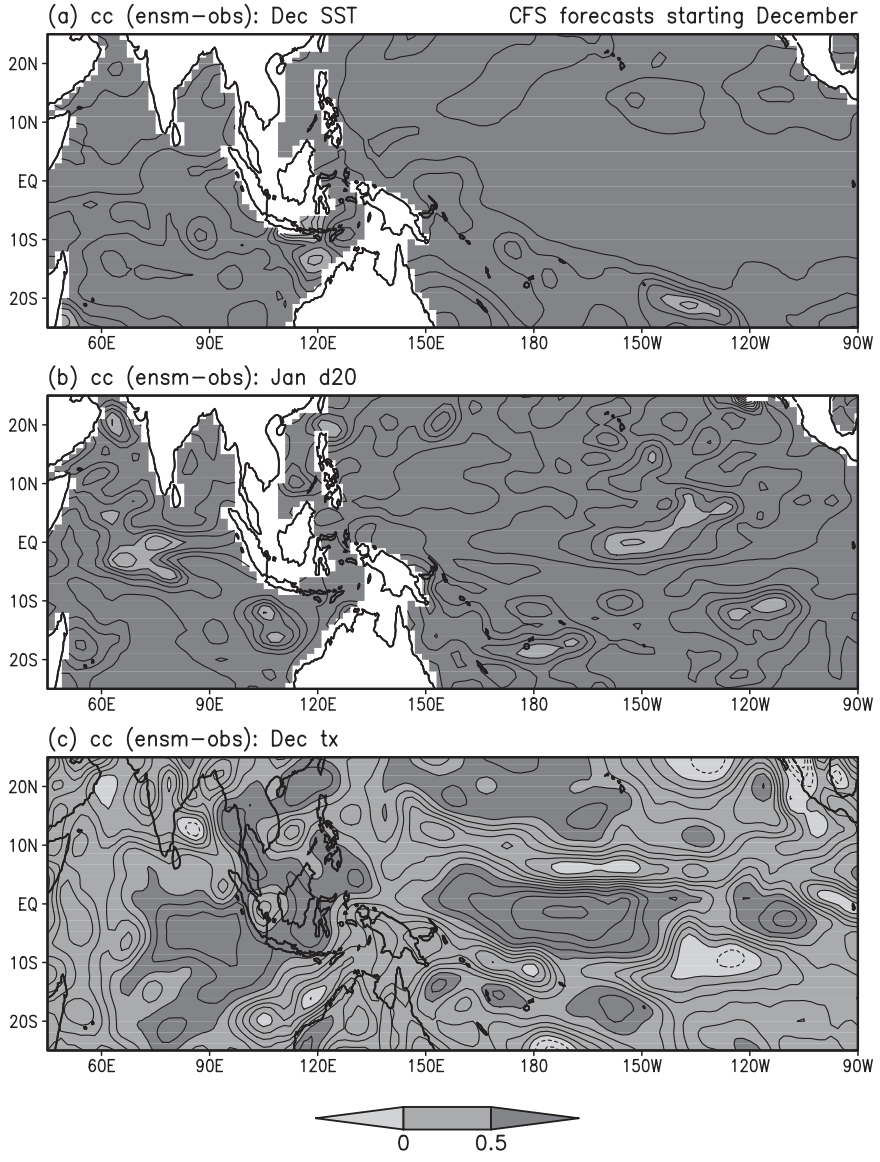

FIG. 3. As in Fig. 2, but from forecasts starting from December.

La Niña anomalies for CFS forecasts and observations. The composites are based on boreal winter Niño-3.4 SST anomalies. Six El Niño events (i.e., 1982/83, 1986/87, 1991/92, 1994/95, 1997/98, and 2002/03) and four La Niña events (i.e., 1984/85, 1988/89, 1998/99, and 1999/2000) are selected for the composites. The December–February Niño-3.4 SST anomalies exceed 1.0°C for these events. Jin and Kinter (2009) have performed similar composites, but for Niño-3 SST.

For observations, the Niño-3.4 SST anomalies decrease quickly in boreal spring (Fig. 5d), consistent with the SST persistence drop. The Niño-3.4 thermocline depth anomalies decay in December–January (Fig. 5e), leading the decrease in the Niño-3.4 SST anomalies by about 4 months. The timing agrees with the first persistence drop in the thermocline depth. The switch of the thermocline depth anomalies around April concurs with the second thermocline depth persistence drop. The western equatorial Pacific zonal wind stress anomalies start to weaken after November (Fig. 5f), which agrees with the drop in the wind stress persistence.

For CFS forecasts, the Niño-3.4 SST anomalies decrease in May–June for forecasts starting from boreal spring (Fig. 5a). For forecasts starting before February, SST anomalies remain large and positive until summer. The timing of decrease in the SST anomalies is consistent with that of the SST persistence drop. The Niño-3.4 thermocline depth anomalies decrease quickly and change

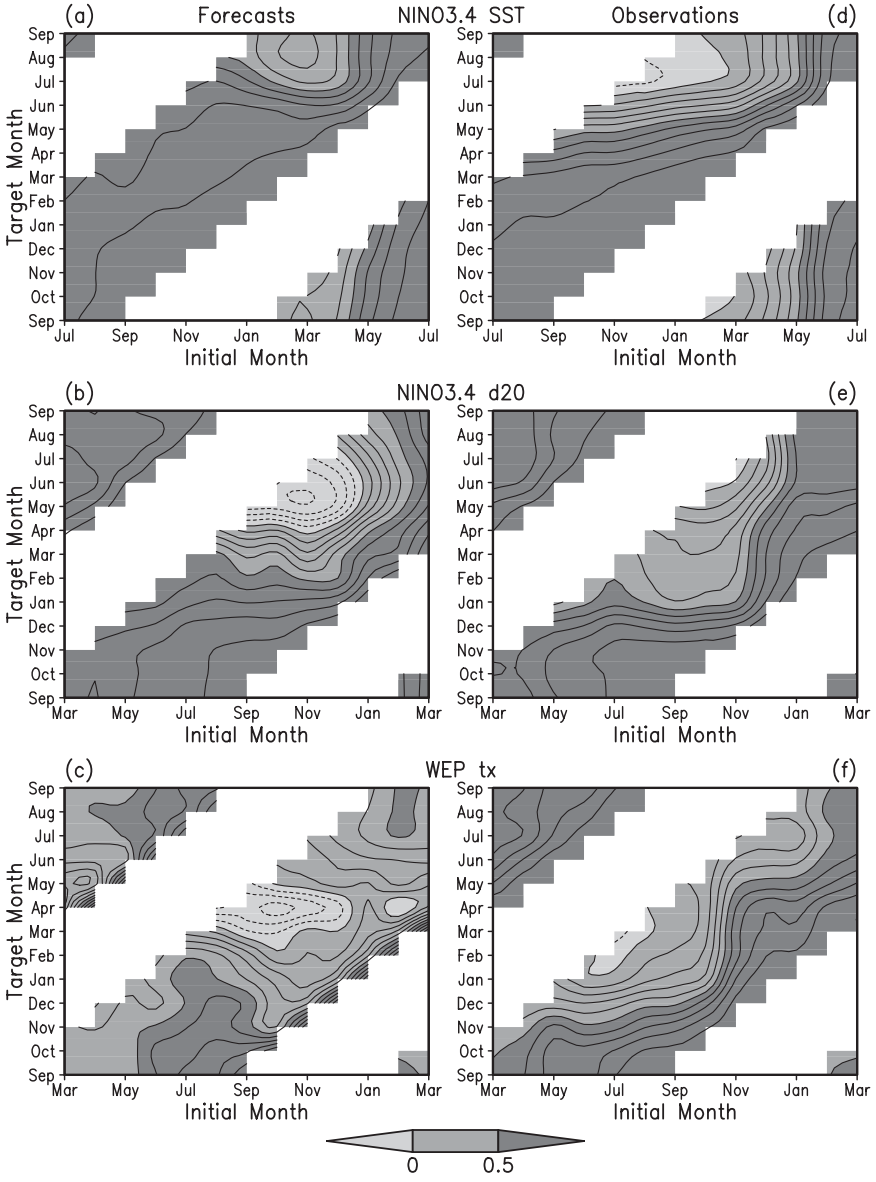

FIG. 4. Auto-lag correlation of anomalies of (a) Niño-3.4 SST, (b) Niño-3.4 thermocline depth, and (c) western equatorial Pacific zonal wind stress derived from CFS individual forecasts. (d)–(f) As in (a)–(c), but from the observations. The CI is 0.1.

sign during February–April for forecasts starting from September to March (Fig. 5b). The forecasts starting from summer display a delay in the timing of decrease in the anomalies. These features agree well with those in the thermocline depth persistence drops. The western equatorial Pacific zonal wind stress anomalies switch sign around February–March for forecasts starting from August to March (Fig. 5c). For forecasts starting from summer, wind stress anomalies remain large westerly in January–February. This feature is also seen in the wind stress auto-lag correlation.

Compared to observations, the CFS forecasts display a delay in the peak and decay time for anomalies of all the three quantities. This delay is more prominent for long-lead forecasts than for short-lead forecasts. The differences in the temporal evolution of these anomalies are consistent with those in the time of the corresponding persistence drops. The decay and phase transition in the western equatorial Pacific zonal wind stress starts about 1 month earlier than that in the Niño-3.4 thermocline depth and the latter, in turn, leads that in the Niño-3.4 SST anomalies by about 4 months. This

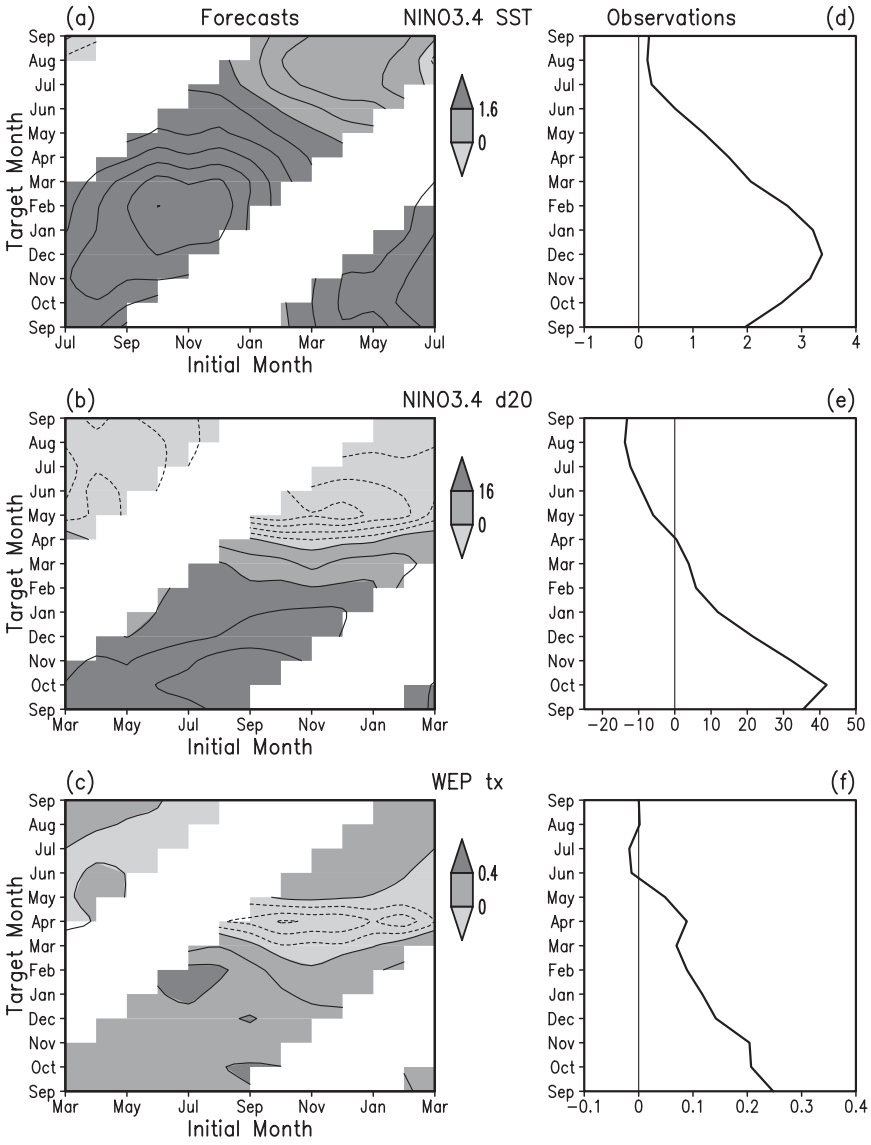

FIG. 5. Anomalies of (a) Niño-3.4 SST (°C), (b) Niño-3.4 thermocline depth (m), and (c) western equatorial Pacific zonal wind stress (dyn cm^{-2}) as differences of the El Niño minus La Niña composite derived from CFS forecasts. (d)–(f) As in (a)–(c), but from observations. The CI for positive (negative) values is 0.4°C (0.2°C) in (a), 8 m (4 m) in (b), and 0.2 dyn cm^{-2} (0.1 dyn cm^{-2}) in (c).

phase relationship is consistent with the time lag among the persistence drops of the three quantities.

Many previous studies have shown that the thermocline depth change is an important factor for the SST evolution, and that the phase transition in the eastern equatorial Pacific SST is preceded by the switch in the thermocline depth (Zebiak and Cane 1987; Balmaseda et al. 1995; Van der Vaart et al. 2000). The thermocline depth change along the equatorial Pacific, in turn, is closely related to surface wind change. The western equatorial Pacific wind anomalies induce oceanic equatorial Kelvin waves that propagate eastward along the equatorial thermocline and change the thermocline depth in the eastern equatorial Pacific. Thus, the eastern equatorial Pacific SST, the equatorial Pacific thermocline depth, and the western equatorial Pacific wind stress anomalies are closely linked together. Because of this link, the phase transition and the persistence barrier for the three are related. A delayed phase transition or persistence barrier in the western equatorial Pacific wind stress will induce a similar delay in the thermocline depth and SST.

c. The seasonal change of variances

Previous studies indicated that the spring barrier of Niño-3 SST concurs with the low variance (Xue et al. 1994). To examine the relation of the persistence barrier to the seasonal change of variance, in Fig. 6 we display the standard deviation of monthly mean Niño-3.4 SST, Niño-3.4 thermocline depth, and the western equatorial Pacific surface zonal wind stress from the CFS forecasts and observations. For the CFS forecasts, the standard deviations are calculated for individual forecasts and the mean values of the 15 standard deviations are shown in Fig. 6.

For observations, the Niño-3.4 SST standard deviation is the smallest during March–July (Fig. 6d) when the SST persistence experiences a large drop. The Niño-3.4 thermocline depth shows two periods of low variance, one in December–January and the other in May, separated by a weak secondary maximum (Fig. 6e). Both periods correspond to decreases in the thermocline depth persistence. For the western equatorial Pacific zonal wind stress, the standard deviation is the smallest during May–July (Fig. 6f), which occurs after the major wind stress persistence barrier. From the previous summer to March, the standard deviation displays an overall increase except for a secondary low value around February. Note that the wind stress variance is the largest in March when the ENSO-related zonal wind stress anomalies are at the decaying phase.

For the CFS forecasts, the Niño-3.4 SST has the smallest standard deviation around May–June (Fig. 6a), which is later than observations. This timing leads that in the SST persistence drop by about 1 month. The Niño-3.4 thermocline depth has the lowest variance in June–July (Fig. 6b), which lags the corresponding persistence drop. For forecasts starting from April to July, a secondary lowest variance appears around December. The western equatorial Pacific zonal wind stress displays the largest standard deviation during February–March (Fig. 6c) when the auto-lag correlation experiences a quick decrease.

From the above results, the relationship between the persistence barrier and the variance differs for different quantities. While the persistence barrier occurs when the variance is low for the Niño-3.4 SST, this is not the case for the Niño-3.4 thermocline depth and the western equatorial Pacific wind stress. For the thermocline depth in the CFS forecasts, the minimum standard deviation occurs after the persistence barrier. For the wind stress in both observations and CFS forecasts, the lowest variance is reached after the persistence barrier. This indicates that the persistence barrier cannot be simply explained by the seasonal change of the variance. This result is consistent with Torrence and Webster (1998).

d. The seasonal change of the signal-to-noise ratio

Another hypothesis for the persistence barrier is the low signal-to-noise ratio (e.g., Torrence and Webster 1998). Here, we examine this hypothesis based on the CFS ensemble forecasts. The noise is estimated by the ensemble spread calculated from the 15 forecasts starting from different initial states. Figure 7 shows the ratio of standard deviation of ensemble mean versus ensemble spread for the three quantities in the CFS forecasts. Note that the ensemble spread is used as a proxy for noise with the view that the larger the ensemble spread the larger the noise. Also, the errors in the standard deviation values enter the noise estimate. This, however, is unlikely to affect our conclusions.

For the Niño-3.4 SST, the lowest signal-to-noise ratio is seen around August–September (Fig. 7a), which is due to both low standard deviation and large spread. The largest spread is observed around August–September when the eastern equatorial Pacific cold tongue is the coldest and the SST front surrounding the cold tongue is the strongest. For the Niño-3.4 thermocline depth, the lowest ratio is seen around March–April for most of the forecasts (Fig. 7b), mainly due to the large spread. For the western equatorial Pacific zonal wind stress, the ratio is the lowest in May for all the forecasts (Fig. 7c), which is mainly due to the small standard deviation.

The temporal relationship between the persistence barrier and the seasonal change of the signal-to-noise ratio indicates that the persistence barrier is unlikely to be explained by the noise variation. In fact, for Niño-3.4 SST, April–June is the time when the noise is the smallest as the equatorial Pacific cold tongue is the weakest. The drop of auto-lag correlations during June–July in the CFS forecasts concurs with the decrease of the signal-to-noise ratio, but not with the lowest ratio. For Niño-3.4 thermocline depth and the western equatorial Pacific zonal wind stress, the auto-lag correlations start to decrease when the spread is increasing and before the signal-to-noise ratio reaches the minimum.

5. Possible reasons for the prediction barrier

Much of the previous literature suggests that the prediction barrier or the persistence barrier is due to the noise. As shown in the previous section, the seasonal change in noise does not entirely explain the persistence barrier. In this section, we investigate whether the noise level plays a role in the prediction barrier, and if not, what is the main reason for the drop of prediction skill.

a. The role of noise

To demonstrate whether the noise contributes to the prediction skill drop, we show in Fig. 8 the correlation

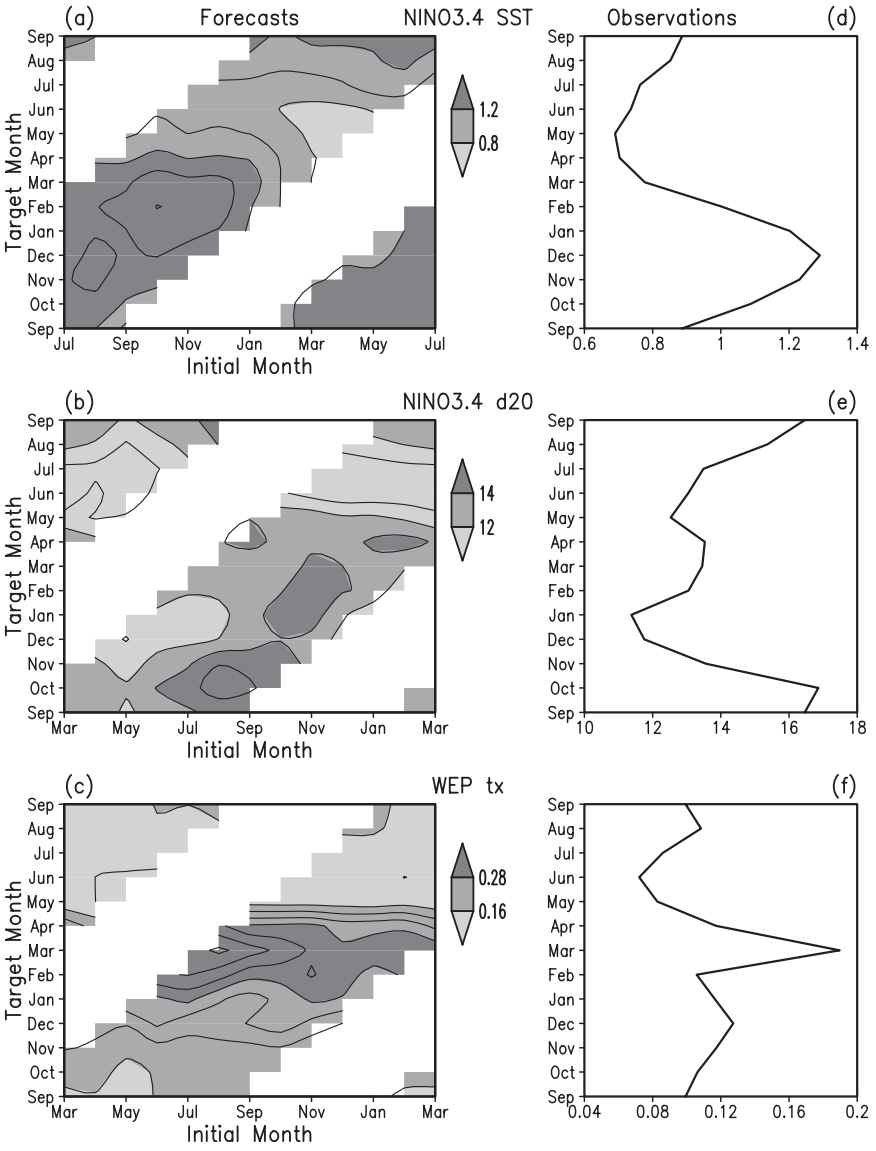

FIG. 6. Std dev of anomalies of (a) Niño-3.4 SST (°C), (b) Niño-3.4 thermocline depth (m), and (c) western equatorial Pacific zonal wind stress (dyn cm^{-2}) derived from CFS forecasts. (d)–(f) As in (a)–(c), but from observations. The CI is 0.2°C in (a), 2 m in (b), and 0.04 dyn cm^{-2} in (c).

skill of three quantities calculated using the ''perfect model approach'' based on the 15-member forecasts. In this calculation, one member of the forecasts is treated as ''observation'' and the ensemble mean of the other 14 members is treated as ''forecast.'' The correlation is calculated for each of the 15 members alternatively treated as observation and Fig. 8 shows the mean of the 15 correlations calculated for Niño-3.4 SST, Niño-3.4 thermocline depth, and the western equatorial Pacific zonal wind stress. In this perfect model approach, the change in the correlation skill is due to the impacts of noise. This is because we have assumed that all the forecasts have the same signal and only differ because of noise. This is a reasonable assumption for modest lead times. At longer leads this assumption may be problematic. Comparison of Figs. 8 and 1 illustrates whether noise contributes to the prediction skill and to what extent.

For Niño-3.4 SST, the lowest predictability is seen during July–September (Fig. 8a), consistent with Saha et al. (2006, their Fig. 3). The skill drop, however, is only about 0.2, much less than that seen in Fig. 1a. In addition,

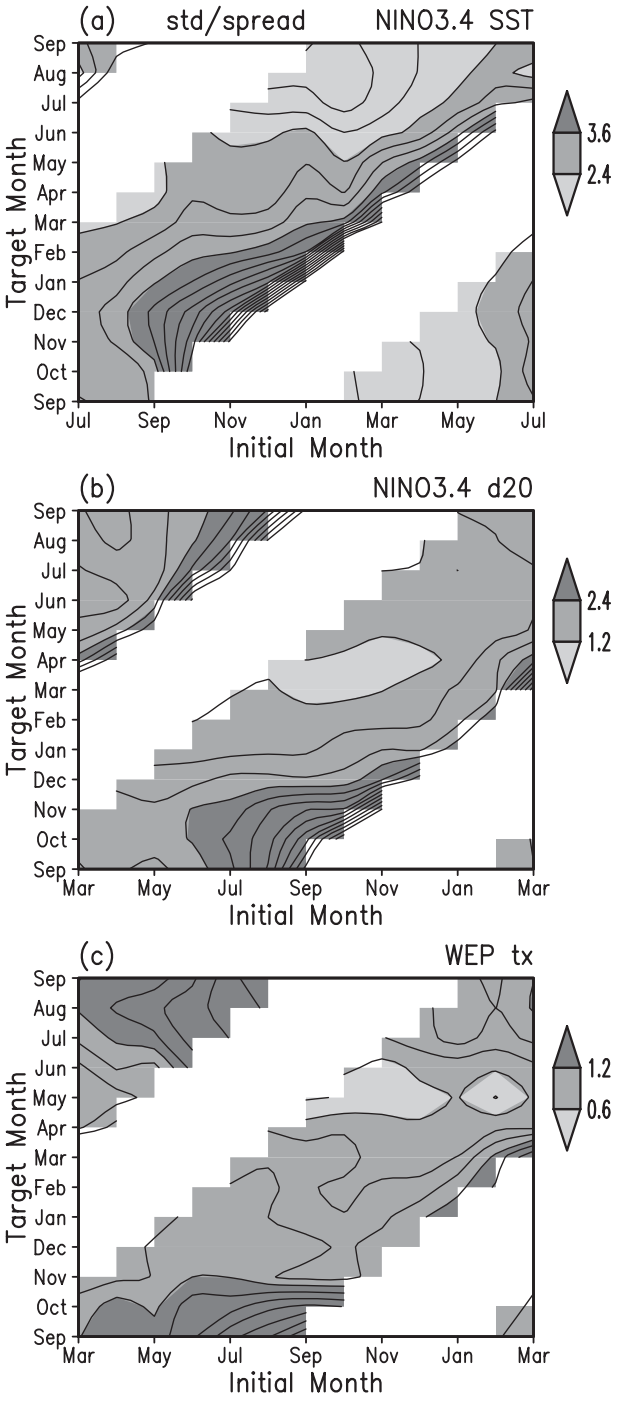

FIG. 7. The ratio of the ensemble mean std dev and the ensemble spread for monthly mean (a) Niño-3.4 SST, (b) Niño-3.4 thermocline depth, and (c) western equatorial Pacific zonal wind stress derived from CFS forecasts. The CI is 0.4 in (a), 0.4 in (b), and 0.2 in (c).

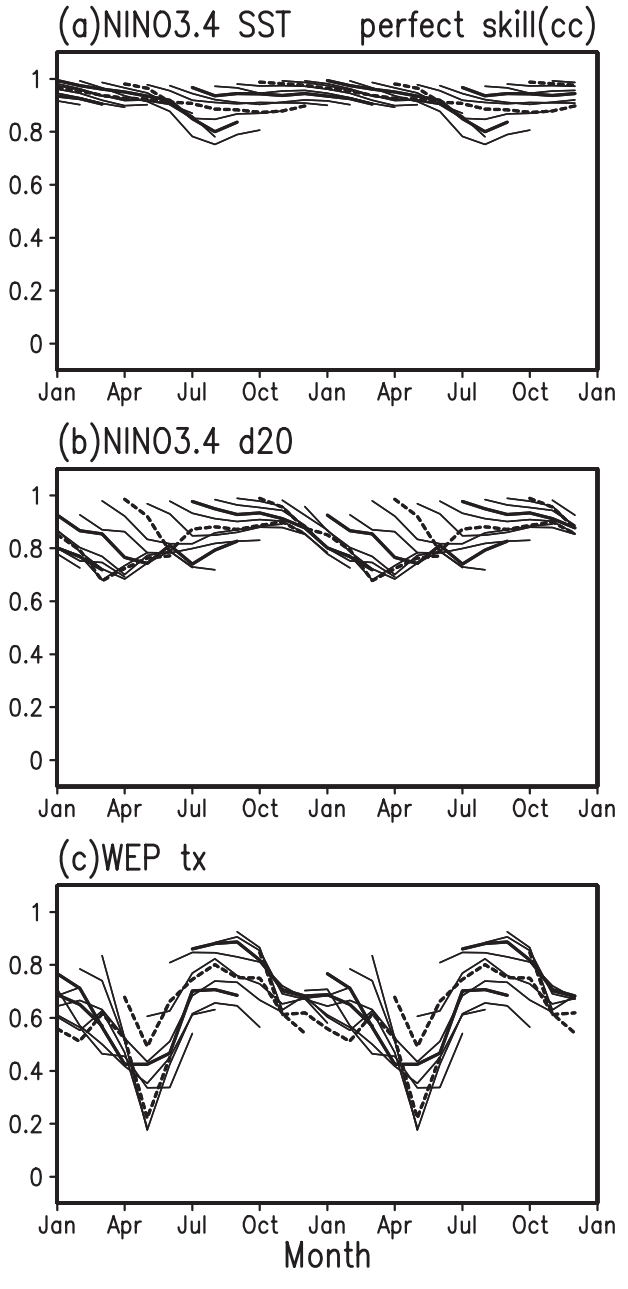

FIG. 8. Correlation skill of (a) Niño-3.4 SST, (b) Niño-3.4 thermocline depth, and (c) western equatorial Pacific zonal wind stress calculated using the perfect model approach from CFS forecasts.

the timing of the skill drop is later than that seen in Fig. 1a. For Niño-3.4 thermocline depth, the skill drop is larger compared to Niño-3.4 SST. The lowest skill is about 0.7 during March–April (Fig. 8b). The low skill in the thermocline depth leads that in the SST by about 4–5 months. For some of the forecasts, there is a secondary correlation minimum in July. Compared to the skill in Fig. 1b, the skill drop is much less and occurs at a later time. For the western equatorial Pacific zonal wind stress, the skill drop is more pronounced, with the lowest correlations occurring around May (Fig. 8c). The skill drop during March–April seems to occur at the same time as the one of the drops seen in Fig. 1c.

The time of the lowest skill appears to be consistent with that of the smallest signal-to-noise ratio. This can be seen by comparing Figs. 8 and 7. All of the perfect model skill minimums occur at the same time as the smallest signal-to-noise ratio. In addition, the secondary correlation minimum in the thermocline depth occurs at the secondary ratio minimum. Furthermore, the amplitude of the drops in correlation also seems to relate to the value of the signal-to-noise ratio. The Niño-3.4 SST maintains a signal-to-noise ratio over 1.2, the Niño-3.4 thermocline depth has the smallest ratio below 1.2, and the western equatorial Pacific zonal wind stress has the smallest ratio below 0.6. It appears that the noise impacts are the largest for the wind stress (perhaps as expected), followed by the thermocline depth, and the SST. This agrees with the differences in the lowest skill induced by noise.

While the above relationship indicates that the noise impacts are closely related to the signal-to-noise ratio, the noise does not entirely explain the prediction skill drops seen in the CFS ensemble forecasts. The question then is, what is responsible for the decline in the prediction skill? Our analyses suggest that the CFS atmospheric (i.e., GFS) wind response to SST anomalies is significantly different from observations, and this difference is amplified by coupled feedback, ultimately leading to the spring prediction barrier. This is demonstrated in the following.

b. Errors in the atmospheric response to SST anomalies

Figure 9 shows the December SST and the surface zonal wind stress anomalies obtained by regression onto the December Niño-3.4 SST for observations and the CFS forecasts from July and December. For the forecasts initialized in December, the SST anomalies in the tropical Indo-Pacific Ocean (Fig. 9e) are in good agreement with the observational estimates (Fig. 9a). The zonal wind stress, however, shows noticeable differences. The anomalous westerly winds over the equatorial central Pacific are larger in the CFS forecasts (Fig. 9f) than in the observations (Fig. 9b). In addition, the westerly winds extend more westward in the forecasts compared to the observations. For the forecasts starting from July, the westward extension of anomalous westerly winds is more obvious (Fig. 9d). This is accompanied by the westward extension of the positive SST anomalies (Fig. 9c).

The differences in the zonal wind stress can affect the ENSO phase transition through ocean–atmosphere coupled processes. Figure 10 shows the temporal evolution of Niño-3.4 SST, Niño-3.4 thermocline depth, Niño-3.4 zonal wind stress, and the western equatorial Pacific zonal wind stress from CFS forecasts starting from December and July and observations, which is obtained by regression with respect to the December Niño-3.4 SST. For forecasts starting from December, the initial month (December) Niño-3.4 SST anomalies are nearly the same in the forecasts and observations (Fig. 10a). The westerly wind stress anomalies, however, are very different. Compared to observations, anomalous westerlies in the Niño-3.4 region are larger throughout the 9-month forecast period (Fig. 10d) and those in the western equatorial Pacific are larger in December (Fig. 10c). The larger westerly anomalies favor the maintaining of positive thermocline depth anomalies in the Niño-3.4 region for a longer period in the CFS forecasts than in observations (Fig. 10b). This leads to a longer persistence of positive SST anomalies in the Niño-3.4 region (Fig. 10a) and, in turn, westerly anomalies over the equatorial central Pacific (Fig. 10d). At the time when observed SST anomalies are near zero, the CFS forecasts still have about 0.5°C positive SST anomalies. As such, low correlation skill appears at the time of observed phase transition.

The differences in the time of the phase transition of the western equatorial Pacific zonal wind stress and the Niño-3.4 thermocline depth anomalies are more clearly seen in the forecasts starting from July. For these forecasts, westerly wind anomalies in the western equatorial Pacific are large and remain so until February, whereas in the observations the westerly anomalies start to decrease quickly around November and become small in February (Fig. 10g). The differences in the Niño-3.4 zonal wind stress anomalies are small before December, but after that these anomalies are larger in the forecasts than in the observations (Fig. 10h). Corresponding to these wind stress differences, the CFS forecasts maintain positive thermocline depth anomalies in the Niño-3.4 region for a longer time, whereas in observations the thermocline depth anomalies become small after December (Fig. 10f). This seems to delay the weakening of positive SST anomalies in the Niño-3.4 region in the forecasts compared to the observations (Fig. 10e). The differences in SST anomalies, in turn, contribute to larger westerly anomalies, in particular, during December–February (Figs. 10g,h).

Another factor that can affect the ENSO phase transition time is the latitudinal structure of the wind stress anomalies. Previous studies have shown that a wider meridional structure in the wind stress response leads to a slower ENSO cycle because the negative feedback due to off-equatorial Rossby waves generated by the wind stress curl needs more time to take effects to turn around ENSO (Kirtman 1997; Van der Vaart et al. 2000; Zelle et al. 2005). Apparently, the tropical Pacific wind

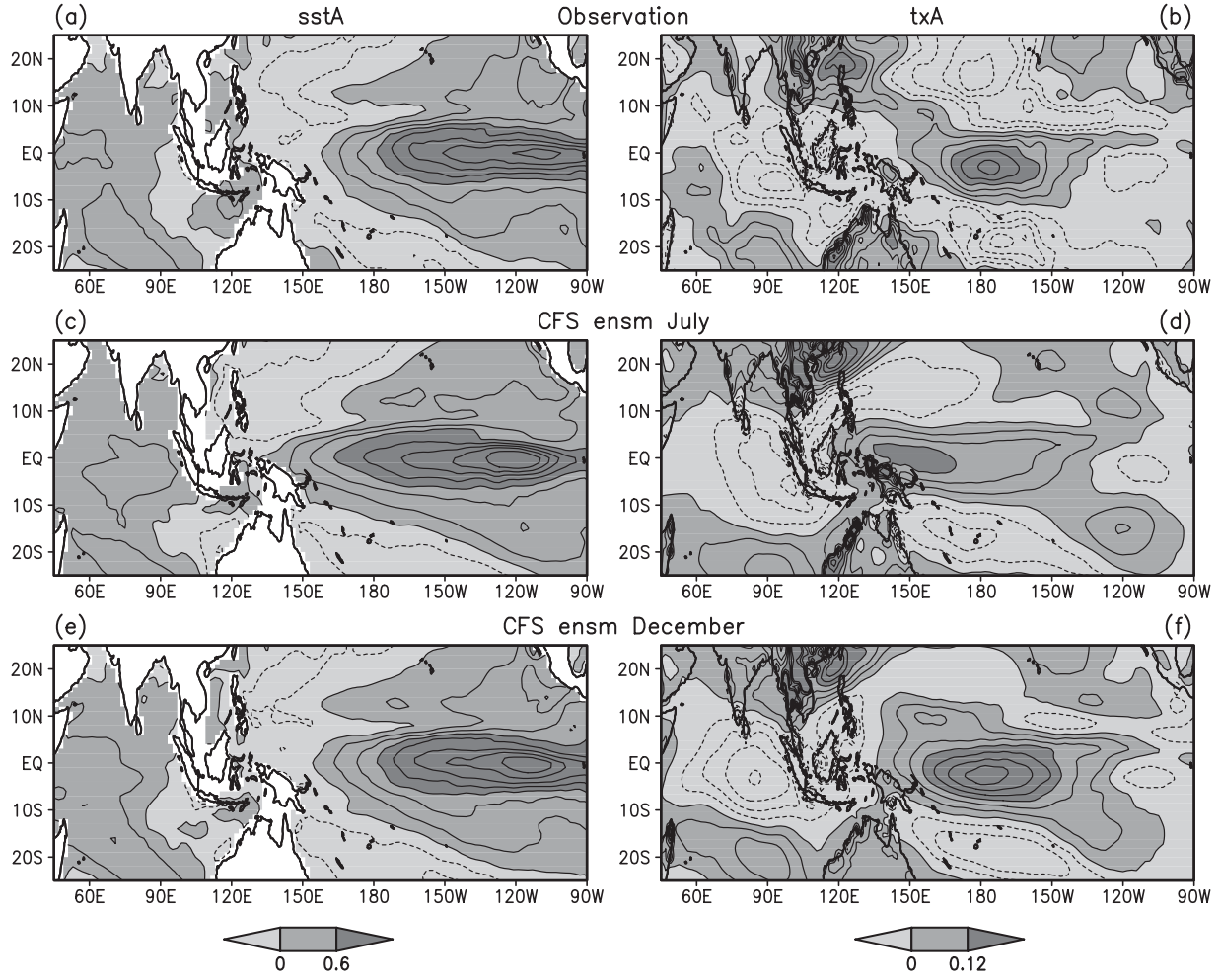

FIG. 9. Anomalies of (a),(c),(e) SST (°C) and (b),(d),(f) zonal wind stress (dyn cm^{-2}) obtained as regression on the December Niño-3.4 SST. (a),(b) Derived from observations. (c),(d) Derived from CFS ensemble mean forecasts starting from July. (e),(f) Derived from CFS ensemble mean forecasts starting from December. The CI is 0.2°C for SST and 0.04 dyn cm^{-2} for wind stress.

stress has a wider latitudinal structure in the model forecasts starting from December (Fig. 9f) compared to the observations (Fig. 9b).

While in the above description we emphasize the wind response to the central-eastern equatorial Pacific SST anomalies, other factors could also contribute to the western equatorial Pacific zonal wind stress. For example, previous studies have indicated the impacts of the eastern Indian Ocean SST (Wu and Kirtman 2004; Terray and Dominiak 2005; Kug et al. 2005; Kug and Kang 2006) and the western North Pacific SST (Weisberg and Wang 1997b; Mayer and Weisberg 1998; Wang et al. 1999) on the western equatorial Pacific winds. As such, improper simulations of SST anomalies in these regions can contribute to the low skill of the western equatorial Pacific wind stress that in turn can affect the prediction skill of the equatorial Pacific thermocline depth and the central-eastern equatorial Pacific SST. Figure 2 indicates that the low wind stress skill is accompanied by the low skill in local SST. Wajsowicz (2007) identified a boreal midwinter prediction barrier of SST in the east pole of the Indian Ocean dipole mode based on analysis of the CFS forecasts. The timing is consistent with that of the western equatorial Pacific winds. Chen et al. (2007) identified a persistence barrier around October and November for SST in the South China Sea during the development phase of strong ENSO cases, which may be linked to the skill drop in the western equatorial Pacific wind stress.

Other plausible factors that may affect the western equatorial Pacific wind changes are the Australian summer monsoon and the western North Pacific monsoon. It is known that the Australian summer monsoon variability is closely related to ENSO (e.g., Hendon 2003; Wu

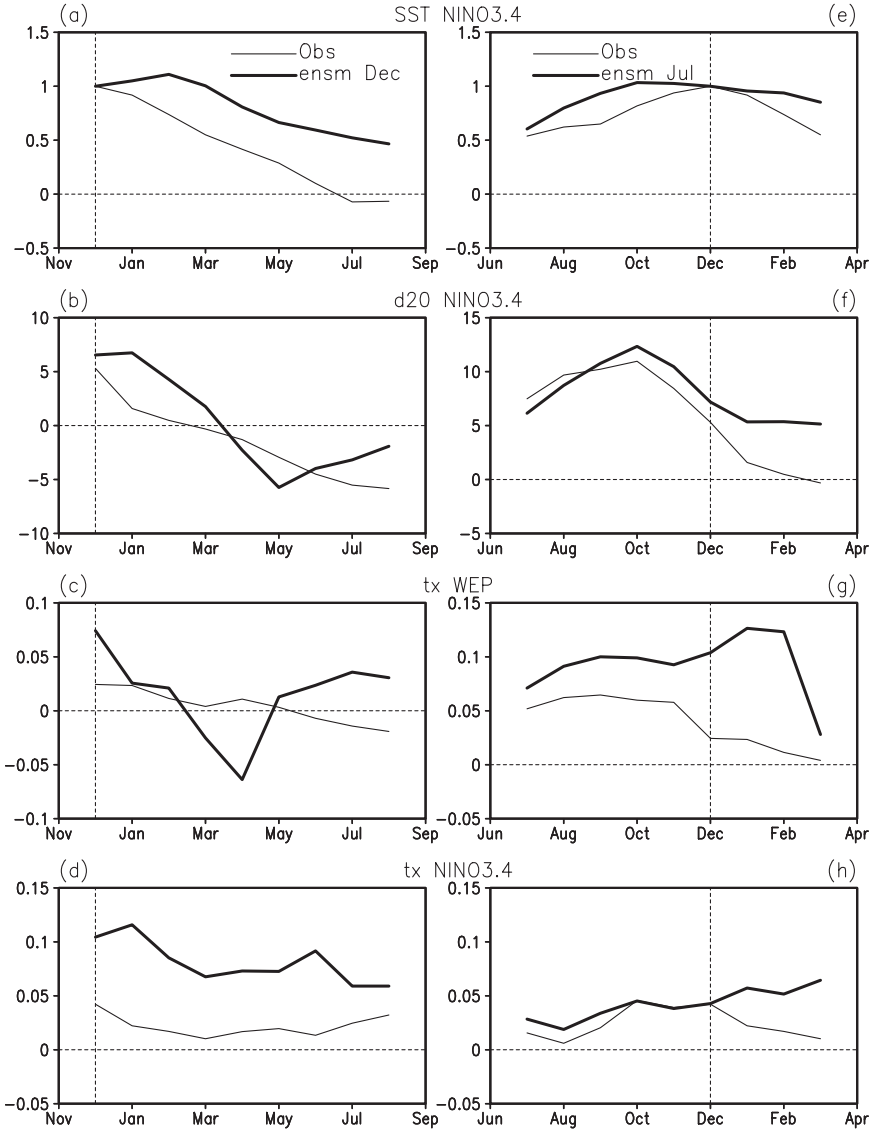

FIG. 10. Anomalies of (a),(e) Niño-3.4 SST (°C); (b),(d) Niño-3.4 thermocline depth (m); (c),(g) western equatorial Pacific zonal wind stress (dyn cm^{-2}); and (d),(h) Niño-3.4 zonal wind stress (dyn cm^{-2}) obtained as regression on the December Niño-3.4 SST. (a)–(d) Derived from observations and CFS ensemble mean forecasts starting from December. (e)–(h) Derived from observations and CFS ensemble mean forecasts starting from July. The thin curves are for observations and the thick curves are for CFS ensemble mean forecasts.

and Kirtman 2007). Large anomalous heating in association with anomalous Australian summer monsoon will induce large wind anomalies over the western equatorial Pacific as a Kelvin wave response (Wu and Kirtman 2007). Similarly, a large anomalous anticyclone (cyclone) develops over the western North Pacific as a remote response to ENSO (Wang et al. 2000, 2003). This anomalous anticyclone (cyclone) can maintain its state through a local air–sea feedback mechanism. To the south of this anomalous anticyclone (cyclone), large zonal wind anomalies develop along the equatorial western Pacific. This indicates that a good forecast for the western equatorial Pacific wind stress depends on the forecast of Australian and western North Pacific monsoons.

6. Summary

The SST, thermocline depth, and surface wind stress over the equatorial Pacific are closely coupled. Previous observational and modeling studies have shown a spring

persistence barrier and model forecasts of ENSO have often encountered a skill drop in boreal spring. The present study documents the prediction and persistence barrier in the CFS retrospective forecasts for SST, thermocline depth, and surface zonal wind stress. It is shown that the CFS retrospective forecasts experience a prominent skill drop in boreal spring for Niño-3.4 SST forecasts, in agreement with Saha et al. (2006), and this is preceded by a skill drop in boreal winter in the Niño-3.4 thermocline depth and the western equatorial Pacific zonal wind stress.

The persistence barriers in the CFS forecasts are delayed compared to observations. The delay is more prominent in long-lead (over 3 months) than short-lead (0–3 month) forecasts. The persistence barrier in the Niño-3.4 SST is preceded by that in the Niño-3.4 thermocline depth and the western equatorial Pacific zonal wind stress for both observations and CFS forecasts. The CFS forecasts capture the time-lag relationship of persistence barriers among the Niño-3.4 SST, Niño-3.4 thermocline depth, and the western equatorial Pacific zonal wind stress.

The time of the persistence barrier agrees well with the time of the phase transition, consistent with previous studies. While the spring barrier of the Niño-3.4 SST is temporally consistent with a period of the lowest variance, this is not the case for the Niño-3.4 thermocline depth and the western equatorial Pacific zonal wind stress. The persistence barrier cannot be entirely explained by the seasonal variation of the noise variance and the signal-to-noise ratio.

Atmospheric noise has a large impact on the prediction skill of the zonal wind stress in boreal spring. However, its effects on the prediction skill in association with ENSO are relatively small with this model. This is consistent with the experiments of Stan and Kirtman (2008) who argued that atmospheric noisiness was not the primary limiting factor in CFS predictability. The analysis presented here shows that in the CFS the atmospheric wind response to ENSO-related SST anomalies is too strong and extends too westward. This deficiency seems to be amplified by coupled processes. As a result, the thermocline depth anomalies actually persist for too long and the ENSO phase transition is delayed in the CFS compared to observations. Our interpretation of this result is that the excessive persistence or delayed phase transition associated with wind stress structural errors is why CFS has a spring prediction barrier. Our results suggest that the spring prediction barrier is largely due to deficiencies in the models, in agreement with Chen et al. (1995) and Jin and Kinter (2009).

Previous studies have shown that the western equatorial Pacific zonal wind stress is an important element in the ENSO evolution (e.g., Weisberg and Wang 1997a,b; Wang et al. 1999). Not surprisingly, the present study indicates that the ENSO prediction skill is closely linked to the wind stress prediction skill. However, we also suggest that by improving the atmospheric model wind stress response to SST anomalies we can expect an improvement in the ENSO forecast skill.

Van Oldenborgh et al. (2005) compared the ENSO prediction skill of the European Centre for Medium-Range Weather Forecasts (ECMWF) model with those of statistical models, albeit the forecasts were only up to 6 months. They found that the ECMWF model does not suffer much from a spring barrier, which seems to suggest that the spring prediction barrier is not an intrinsic property of the system. It would be very useful to examine whether the ECMWF model also does not suffer from overly large systematic biases in the atmospheric wind response to ENSO and the overly persistence of SST, which is, however, beyond the scope of the present study.

Acknowledgments. The authors appreciate the comments of Wanqiu Wang, Geert Jan van Oldenborgh, and an anonymous reviewer. This research was supported by NSF Grant ATM-0332910, NOAA Grants NA04OAR4310034 and NA05OAR4311135, and NASA Grant NNG04GG46G.

REFERENCES

Balmaseda, M. A., D. L. T. Anderson, and M. K. Davey, 1994: ENSO prediction using a dynamical ocean model coupled to statistical atmospheres. *Tellus,* **46A,** 497–511.

——, M. K. Davey, and D. L. T. Anderson, 1995: Decadal and seasonal dependence of ENSO prediction skill. *J. Climate,* **8,** 2705–2715.

Barnston, A. G., and Coauthors, 1994: Long-lead seasonal forecasts—Where do we stand? *Bull. Amer. Meteor. Soc.,* **75,** 2097–2114.

Blumenthal, M. B., 1991: Predictability of a coupled ocean–atmosphere model. *J. Climate,* **4,** 766–784.

Branstator, G., 1986: The variability in skill of 72-hour global-scale NMC forecasts. *Mon. Wea. Rev.,* **114,** 2628–2639.

Burgers, G., F.-F. Jin, and G. J. van Oldenborgh, 2005: A simplest ENSO recharge oscillator. *Geophys. Res. Lett.,* **32,** L13706, doi:10.1029/2005GL022951.

Carton, J. A., G. Chepurin, X. Cao, and B. Geise, 2000: A simple ocean data assimilation analysis of the global upper ocean 1950–95. Part I: Methodology. *J. Phys. Oceanogr.,* **30,** 294–309.

Chen, D., S. E. Zebiak, A. J. Busalacchi, and M. A. Cane, 1995: An improved procedure for El Niño forecasting. *Science,* **269,** 1699–1702.

——, ——, M. A. Cane, and A. J. Busalacchi, 1997: Initialization and predictability of a coupled ENSO forecast model. *Mon. Wea. Rev.,* **125,** 773–788.

Chen, J.-M., T. Li, and C.-F. Shih, 2007: Fall persistence barrier of sea surface temperature in the South China Sea associated with ENSO. *J. Climate,* **20,** 158–172.

Clarke, A. J., and S. Van Gorder, 1999: The connection between the boreal spring Southern Oscillation persistence barrier and biennial variability. *J. Climate,* **12,** 612–620.

——, and L. Shu, 2000: Quasi-biennial winds in the far western equatorial Pacific phase-locking El Niño to the seasonal cycle. *Geophys. Res. Lett.,* **27,** 771–774.

DeWitt, D. G., 2005: Retrospective forecasts of interannual sea surface temperature anomalies from 1982 to present using a directly coupled atmosphere–ocean general circulation model. *Mon. Wea. Rev.,* **133,** 2972–2995.

Goldenberg, S. B., and J. J. O'Brien, 1981: Time and space variability of tropical Pacific wind stress. *Mon. Wea. Rev.,* **109,** 1190–1207.

Goswami, B. N., and J. Shukla, 1991: Predictability of a coupled ocean–atmosphere model. *J. Climate,* **4,** 3–22.

Hendon, H. H., 2003: Indonesia rainfall variability: Impacts of ENSO and local air–sea interaction. *J. Climate,* **16,** 1775–1790.

Jin, E. K., and J. L. Kinter III, 2009: Characteristics of tropical Pacific SST predictability in coupled GCM forecasts using the NCEP CFS. *Climate Dyn.,* **32,** 675–691, doi:10.1007/s00382-008-0418-2.

——, and Coauthors, 2008: Current status of ENSO prediction skill in coupled ocean–atmosphere models. *Climate Dyn.,* **31,** 647–664.

Kanamitsu, M., W. Ebisuzaki, J. Woollen, S.-K. Yang, J. J. Hnilo, M. Fiorino, and G. L. Potter, 2002: NCEP–DOE AMIP-II Reanalysis (R-2). *Bull. Amer. Meteor. Soc.,* **83,** 1631–1643.

Kirtman, B. P., 1997: Oceanic Rossby wave dynamics and the ENSO period in a coupled model. *J. Climate,* **10,** 1690–1705.

——, J. Shukla, B. Huang, Z. Zhu, and E. K. Schneider, 1997: Multi-seasonal prediction with a coupled tropical ocean–global atmosphere system. *Mon. Wea. Rev.,* **125,** 789–808.

——, ——, M. Balmaseda, N. Graham, C. Penland, Y. Xue, and S. Zebiak, 2001: Current status of ENSO forecast skill: A report to the Climate Variability and Predictability (CLIVAR) Numerical Experimentation Group (NEG). WCRP Informal Rep. 23/01, 31 pp. [Available online at http://www.clivar.org/publications/wg_reports/wgsip/nino3/report.htm.]

Kug, J.-S., and I.-S. Kang, 2006: Interactive feedback between ENSO and the Indian Ocean. *J. Climate,* **19,** 1784–1801.

——, S.-I. An, F.-F. Jin, and I.-S. Kang, 2005: Preconditions for El Niño and La Niña onsets and their relation to the Indian Ocean. *Geophys. Res. Lett.,* **32,** L05706, doi:10.1029/2004GL021674.

Latif, M., and Coauthors, 1998: A review of the predictability and prediction of ENSO. *J. Geophys. Res.,* **103,** 14 375–14 393.

Lau, K.-M., and S. Yang, 1996: The Asian monsoon and predictability of the tropical ocean–atmosphere system. *Quart. J. Roy. Meteor. Soc.,* **122,** 945–957.

Mayer, D. A., and R. H. Weisberg, 1998: El Niño-Southern Oscillation-related ocean–atmosphere coupling in the western equatorial Pacific. *J. Geophys. Res.,* **103** (C9), 18 635–18 648.

McPhaden, M. J., 2003: Tropical Pacific Ocean heat content variations and ENSO persistence barriers. *Geophys. Res. Lett.,* **30,** 1480, doi:10.1029/2003GL016872.

——, and Coauthors, 1998: The Tropical Ocean–Global Atmosphere observing system: A decade of progress. *J. Geophys. Res.,* **103** (C7), 14 169–14 240.

Meinen, C. S., and M. J. McPhaden, 2000: Observations of warm water volume changes in the equatorial Pacific and their relationship to El Niño and La Niña. *J. Climate,* **13,** 3551–3559.

Moore, A. M., and R. Kleeman, 1996: The dynamics of error growth and predictability in a coupled model of ENSO. *Quart. J. Roy. Meteor. Soc.,* **122,** 1405–1446.

Moorthi, S., H.-L. Pan, and P. Caplan, 2001: Changes to the 2001 NCEP operational MRF/AVN global analysis/forecast system. Technical Procedures Bulletin 484, NWS Office of Meteorology, 14 pp. [Available online at http://www.weather.gov/om/tpb/484.pdf.]

Neelin, J. D., M. Latif, and F.-F. Jin, 1994: Dynamics of coupled ocean–atmosphere models: The tropical problem. *Annu. Rev. Fluid Mech.,* **26,** 617–659.

Pacanowski, R. C., and S. M. Griffies, 1998: MOM 3.0 manual. NOAA/Geophysical Fluid Dynamics Laboratory, 638 pp.

Philander, S. G. H., 1990: *El Niño, La Niña and the Southern Oscillation*. Academic Press, 293 pp.

Reynolds, R. W., N. A. Rayner, T. M. Smith, D. C. Stokes, and W. Wang, 2002: An improved in situ and satellite analysis for climate. *J. Climate,* **15,** 1609–1625.

Saha, S., and Coauthors, 2006: The NCEP Climate Forecast System. *J. Climate,* **19,** 3483–3517.

Schneider, E. K., D. G. DeWitt, A. Rosati, B. P. Kirtman, L. Ji, and J. J. Tribbia, 2003: Retrospective ENSO forecasts: Sensitivity to atmospheric model and ocean resolution. *Mon. Wea. Rev.,* **131,** 3038–3060.

Smith, T., A. G. Barnston, M. Ji, and M. Chelliah, 1995: The impact of Pacific Ocean subsurface data on operational prediction of tropical Pacific SST at the NCEP. *Wea. Forecasting,* **10,** 708–714.

Stan, C., and B. P. Kirtman, 2008: The influence of atmospheric noise and uncertainty in ocean initial conditions on the limit of predictability in a coupled GCM. *J. Climate,* **21,** 3487–3503.

Terray, P., and S. Dominiak, 2005: Indian Ocean sea surface temperature and El Niño–Southern Oscillation: A new perspective. *J. Climate,* **18,** 1351–1368.

Torrence, C., and P. J. Webster, 1998: The annual cycle of persistence in the El Niño/Southern Oscillation. *Quart. J. Roy. Meteor. Soc.,* **124,** 1985–2004.

Troup, A. J., 1965: The ''Southern Oscillation.'' *Quart. J. Roy. Meteor. Soc.,* **91,** 490–506.

Van den Dool, H. M., and Z. Toth, 1991: Why do forecasts for ''near normal'' often fail? *Wea. Forecasting,* **6,** 76–85.

Van der Vaart, P. C. F., H. A. Dijkstra, and F. F. Jin, 2000: The Pacific cold tongue and the ENSO mode: A unified theory within the Zebiak–Cane model. *J. Atmos. Sci.,* **57,** 967–988.

Van Oldenborgh, G. J., M. A. Balmaseda, L. Ferranti, T. N. Stockdale, and D. L. T. Anderson, 2005: Did the ECMWF seasonal forecast model outperform statistical ENSO forecasts models over the last 15 years? *J. Climate,* **18,** 3240–3249.

Wajsowicz, R. C., 2007: Seasonal-to-interannual forecasting of tropical Indian Ocean sea surface temperature anomalies: Potential predictability and barriers. *J. Climate,* **20,** 3320–3343.

Wang, B., R. Wu, and R. Lukas, 1999: Roles of the western North Pacific wind variation in thermocline adjustment and ENSO phase transition. *J. Meteor. Soc. Japan,* **77,** 1–16.

——, ——, and X. Fu, 2000: Pacific–East Asian teleconnection: How does ENSO affect East Asian climate? *J. Climate,* **13,** 1517–1536.

——, ——, and T. Li, 2003: Atmosphere–warm ocean interaction and its impacts on the Asian–Australian monsoon variation. *J. Climate,* **16,** 1195–1211.

Wang, W., S. Saha, H.-L. Pan, S. Nadiga, and G. White, 2005: Simulation of ENSO in the new NCEP Coupled Forecast System Model (CFS03). *Mon. Wea. Rev.,* **133,** 1574–1593.

Webster, P. J., 1995: The annual cycle and predictability of the tropical coupled ocean–atmosphere system. *Meteor. Atmos. Phys.,* **56,** 33–55.

——, and S. Yang, 1992: Monsoon and ENSO: Selectively interactive systems. *Quart. J. Roy. Meteor. Soc.,* **118,** 877–926.

Weisberg, R. H., and C. Wang, 1997a: Slow variability in the equatorial west-central Pacific in relation to ENSO. *J. Climate,* **10,** 1998–2017.

——, and ——, 1997b: A western Pacific oscillator paradigm for the El Niño–Southern Oscillation. *Geophys. Res. Lett.,* **24,** 779–782.

Wright, P. B., 1985: The Southern Oscillation: An ocean–atmosphere feedback system? *Bull. Amer. Meteor. Soc.,* **66,** 398–412.

Wu, R., and B. P. Kirtman, 2004: Understanding the impacts of the Indian Ocean on ENSO variability in a coupled GCM. *J. Climate,* **17,** 4019–4031.

——, and ——, 2007: Roles of the Indian Ocean in the Australian summer monsoon–ENSO relationship. *J. Climate,* **20,** 4768–4788.

——, ——, and K. Pegion, 2006: Local air–sea relationship in observations and model simulations. *J. Climate,* **19,** 4914–4932.

Xue, Y., M. A. Cane, S. E. Zebiak, and M. B. Blumenthal, 1994: On the prediction of ENSO: A study with a low-order Markov model. *Tellus,* **46A,** 512–528.

——, A. Leetmaa, and M. Ji, 2000: ENSO prediction with Markov models: The impact of sea level. *J. Climate,* **13,** 849–871.

Yu, J.-Y., 2005: Enhancement of ENSO's persistence barrier by biennial variability in a coupled atmosphere–ocean general circulation model. *Geophys. Res. Lett.,* **32,** L13707, doi:10.1029/2005GL023406.

Zebiak, S. E., 1989: Ocean heat content variability and ENSO cycle. *J. Phys. Oceanogr.,* **19,** 475–485.

——, and M. A. Cane, 1987: A model El Niño–Southern Oscillation. *Mon. Wea. Rev.,* **115,** 2262–2278.

Zelle, H., G. J. van Oldenborgh, G. Burgers, and H. Dijkstra, 2005: El Niño and greenhouse warming: Results from ensemble simulations with the NCAR CCSM. *J. Climate,* **18,** 4669–4683.